

## Development of A 3d Model Eddy Current Testing

Aber Chifaa<sup>1</sup>, Hamid Azzedine<sup>2</sup>, Elchikh Mokhtar<sup>3</sup>, Lebey Thierry<sup>4</sup>

<sup>1,3</sup>(Physics Department, University Of Science And Technology USTO, Oran, Algeria)

<sup>2</sup>(Faculty Of Electrical Engineering, USTO-MB Oran University, Algeria)

<sup>4</sup>(University Paul Sabatier, Toulouse Cedex 9, France)

**Abstract:** The main stake is to detect a defective component or likely to become it during manufacture or in-service inspections, while improving control productivity. In this context, we develop a simulation tool of EC fastened structures testing, integrated to the ANSYS platform, aimed at conceiving testing methods, optimizing and qualifying it. The finite element method has been chosen, it is suitable for this type of problem. Various configurations have been considered for the inspection of a target with a defect in different thicknesses. Due to the impossibility to detect a defect located at a distance much greater than the skin depth  $\delta$ . Indeed, the eddy currents amplitude are less than 95% of the maximum amplitude beyond a depth greater than  $3 \delta$ . We are interested in the detection of defects located at depths higher to three times the skin depth.

**Keywords:** Eddy current, Finite element method, NDT, Defect characterization, Numerical analysis.

### I. Introduction

Eddy current testing is one of the most extensively used non-destructive testing techniques for inspecting electrically conductive materials at very high speeds without requirement of any contact between the test piece and the sensor [1]. This technique is used to detect defects (cracks, corrosion, etc.) in conducting materials. By inducing alternating electromagnetic fields near the material under investigation, eddy currents start to flow because of the conductivity. The objective of this paper is to study the detection of defects in a conductive target. The successful use of the finite element method for analysis and follow awkward shapes, and the relative economy of computer facilities make it a particularly attractive method for modeling of electromagnetic NDT phenomena. The parameters studied are the impedance change of the sensor, the magnetic flux density and the distribution of eddy currents

[2..6] Which undergo variations in the presence of defects. We considered the following cases: open defect, defect in the skin depth, deep defect and very deep defect (greater than 3 times the skin depth). the model used can also inform us about the depth of a defect [7..12].

### II. Description of the problem

The geometry of the problems considered is illustrated schematically in Fig.1. An axisymmetric air-core coil with an inner coil radius of  $r_1 = 6.5\text{mm}$  and external  $r_2 = 12.5\text{mm}$  and height  $h = 6.5\text{mm}$  placed above the evaluated plate with a magnetic permeability  $\mu_0 = 4\pi \cdot 10^{-7}$ , resistivity  $\rho = 1.7 \cdot 10^{-8} \Omega \cdot \text{m}$ , and lift-off  $l_0 = 0.5\text{mm}$ .

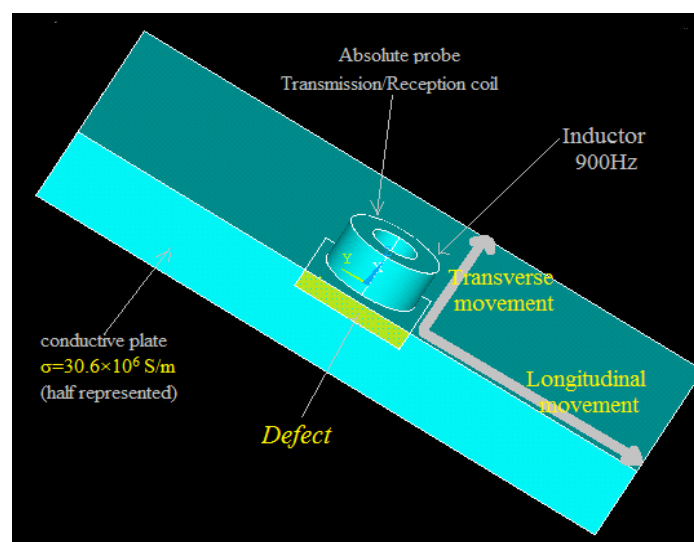


Fig.1: Design of the sensor's coil and the piece used in 3D.

The forward problem consists in the determination of the crack in the plate by the variation of the probe impedance. The impedance change of the coil reflects the change in conductivity distribution in a test specimen in the presence of defects.

## II. Formulation Of The Problem

The differential equation governing eddy current phenomena in regions that include conducting and magnetic materials [13-14] can be written as

$$\frac{1}{\mu}(\nabla \times \nabla \times \bar{A}) = \bar{J}_s - \sigma \frac{\partial \bar{A}}{\partial t} \quad (1)$$

With boundary condition of type Dirichlet on the borders:

$$\bar{A} = \vec{0} \text{ on the borders} \quad (2)$$

Where  $\bar{A}$  is the magnetic vector potential,  $\mu$  is the magnetic permeability (H/m),  $A$  the magnetic vector potential (wb/m),  $\bar{J}_s$  the applied current density vector in the coil ( $A/m^2$ ), and  $\sigma$  is the material conductivity. Solution to this linear diffusion equation for the sinusoidal steady-state condition can be obtained in terms of  $A$  by solving “(1)” with appropriate boundary condition. From the value of  $A$ , one can obtain any observable electromagnetic phenomena such as coil impedance changes, energy dissipation, flux densities, etc. Many practical eddy current geometries are axisymmetric as the excitation coils are circular. Hence, Equation (1) reduces to

$$\frac{1}{\mu} \left( \frac{\partial^2 \bar{A}}{\partial r^2} + \frac{1}{r} \frac{\partial \bar{A}}{\partial r} + \frac{\partial^2 \bar{A}}{\partial z^2} - \frac{\bar{A}}{r^2} \right) = -\bar{J}_s + j\omega\sigma\bar{A} \quad (3)$$

The finite element method does not offer a solution to the diffusion equation directly. Instead, the solution is obtained at discrete points (nodes) in the solution region by formulating an energy functional equivalent to “(3)” and minimizing it with respect to an approximate function space, thus solving the resulting simultaneous algebraic equations for the unknown magnetic vector potential values at each point in the region.

### Impedance of eddy current coils

In NDT application, the signals from eddy current probes carry information concerning the environment of the probes, changes in which cause variations in the probe impedance. The coil impedance can be calculated directly from the complex magnetic vector potential. The impedance of a circular loop of radius  $r_i$  carrying a current  $I_s$  is

$$\bar{Z}_i = \frac{j\omega 2\pi \bar{A}_i r_i}{I_s} \quad (4)$$

Where  $\bar{A}_i$  is the value of the magnetic vector potential at  $r_i$ . Integration of this equation over the cross section of the coil yields the impedance of the coil. Because the values of  $A$  are not known at the location of each turn in the coil, an average value is taken as representing the magnetic vector potential in each element. This value is associated with the centroid of the element, the radius of the loop being  $r_c$ . Then, the impedance of the coil is

$$Z_{coil} = - \frac{j\omega 2\pi J_s}{I_s^2} \sum_{j=1}^N (r_{ci} A_j) A_{cj} \quad (5)$$

Where  $N$  is the number of elements in the cross section of the coil.

### Calculation of inductances and impedances from energy considerations

The impedance of a source can be calculated from the energy of the system by associating its inductance with the stored energy and its resistance with dissipated energy. Thus in “(3)” the left-hand side represents the stored energy in the magnetic field, while the second term on the right-hand side is the eddy

current density and therefore represents the dissipated energy [15-16]. The stored energy can be expressed as a volume integral:

$$W = \frac{1}{2} \int_v B.H dv \quad (6)$$

The inductance of the source, regardless of its shape and distribution, can be written as

$$L = 2W / I_s^2 \quad (7)$$

Where  $I_s$  is the current in the coil.

The calculation of the resistive part of the system is based on the eddy current distribution. The power dissipated in a conducting solid body under the influence of a time-harmonic electromagnetic field is

$$P = \frac{1}{2} \int_{vol} \rho |\overline{J_t}|^2 dv \quad (8)$$

The source resistance now becomes

$$R = P / I_s^2 \quad (9)$$

### III. Finite Element Modeling

The FEM program was written using the developed APDL program with conjunction with Matlab. Four regions are formed according to the problem geometry. The first element is the circular air-core coil, the second element is the tested piece, the third is the crack and the last one is the air domain. The coil displacement increases from -100 to 100 mm, with a step of 10mm for each simulation. The FEM was based on a discrete domain which has a number of elements. Mesh was generated with hexahedral elements.

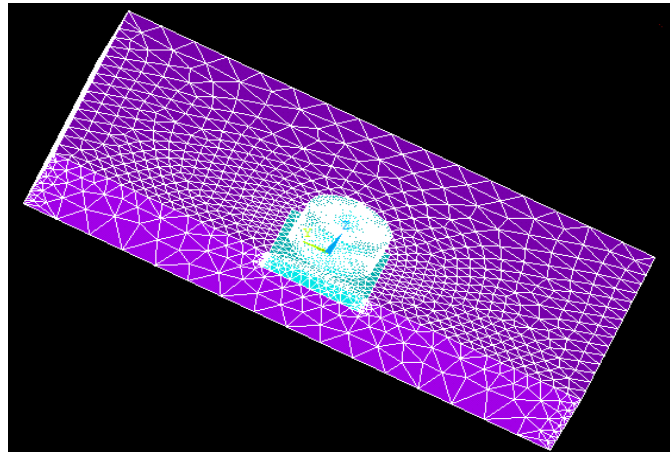


**Fig.2:** Meshing sensor and plate in Ansys14.0

#### IV.1. Eddy current density distribution

In absolute mode, we must perform two simulations: a first configuration with defect and a second flawless. However, it retains exactly the same geometry and the same mesh, only the "defect" zone of the material differs between the two simulations.

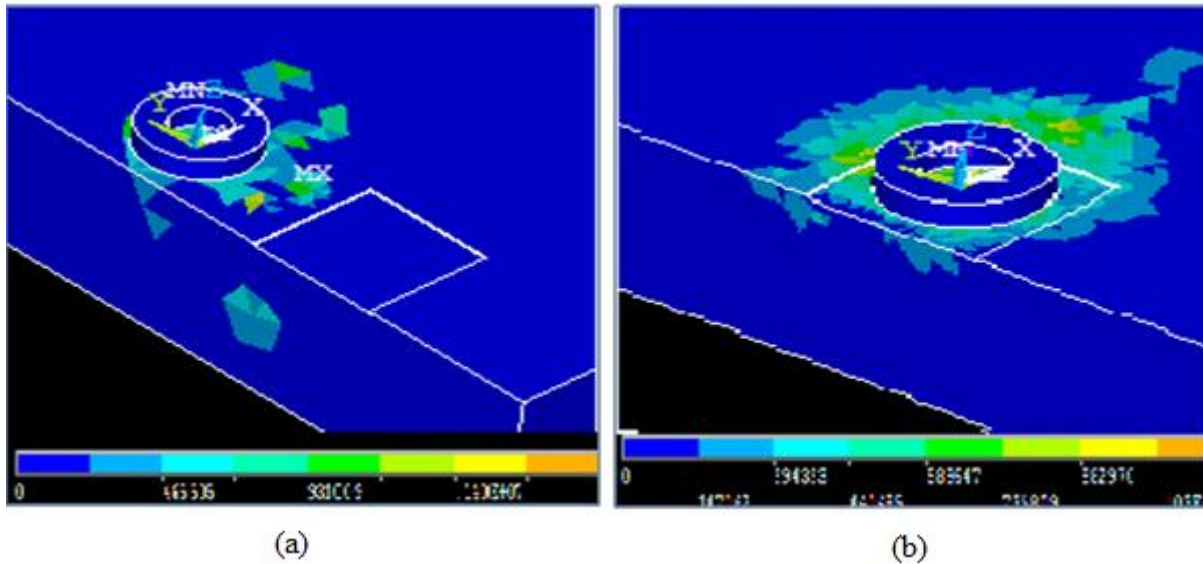


**Fig.3:** Defect influence on eddy current densities  
 (a) coil out of the defect, (b) coil on the defect.

**IV.2. Impedance change**

The sensor has been moved over the specimen with a distance of a 10 mm step-by-step along x axes. The impedance change is because of the presence of the flaw. The impedance values are calculated twice: with and without the crack. The difference of these two values was the impedance change. The plotted values are the impedance change due to the crack as a function of displacement. The results are quite satisfactory:

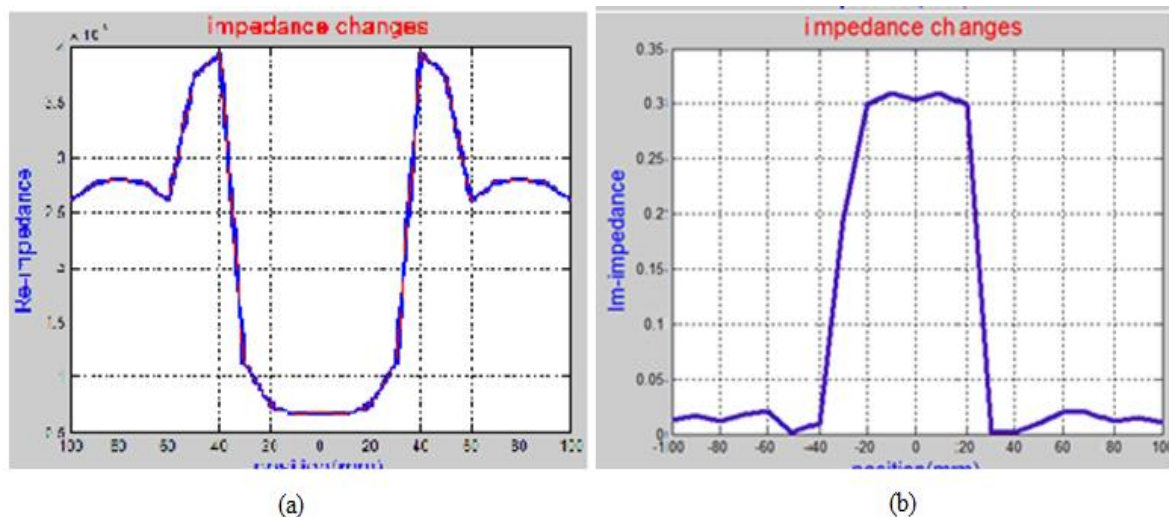


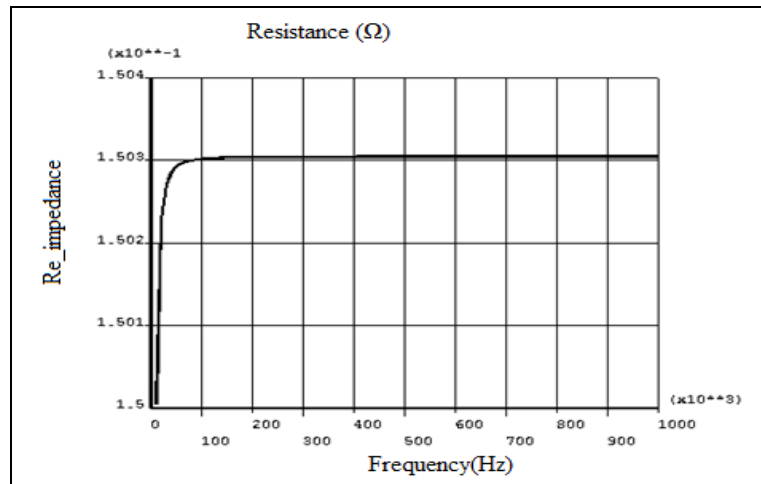
**Fig.4:** Defect influence on impedance changes  
 (a) Real part. (b) Imaginary part.

**IV. 3. Determination of optimum excitation frequency**

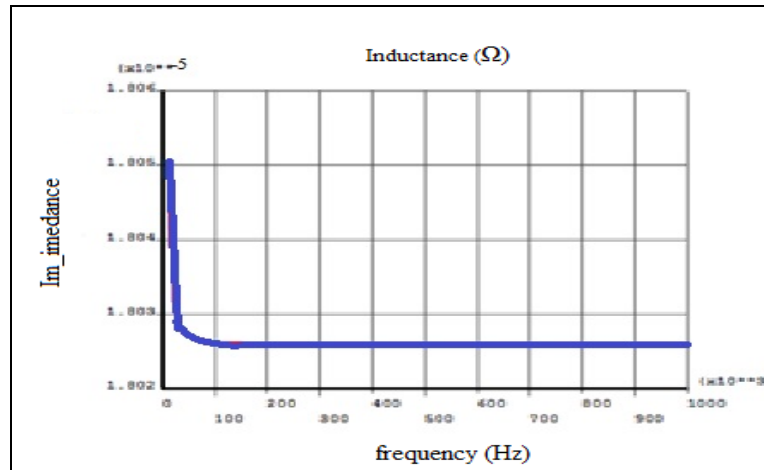
As the frequency of the transmission stream is a predominant factor in the intensity of the EC and the skin depth, it strongly affects the detection performance. The modeling must take into account physical phenomena associated with the sensor working frequencies [17].

The main phenomena that may occur include the skin effect, proximity effect and the parasitic capacitance inter turn. Fig (5) presents a simulation of the impedance of the coil for the presence of the test plate in the range of frequencies between 100Hz and 1MHz. The resistance is influenced by the proximity effect and the currents induced in the test plate. To reel in vacuum resistance is influenced only by the proximity effect which is more apparent at 10 kHz. In the presence of the test plate, the eddy currents developed in the latter affect the resistance of the coil even at low frequencies.

The fall of the equivalent inductance and the rise of the equivalent resistance is due to the fact that high-frequency currents are changing only on the edges of the conductors (in skin depth) and therefore the wire cross-section view of the current is lower.



(a)



(b)

**Fig.5:** Impedance of the sensor as a function of frequency for modeling in the presence of the defect.  
**(a)** Resistance. **(b)** Inductance.

#### IV.4. Cases of application

To test the behavior of our model in different configurations, we set the frequency and we simulate the case of defect at several depths (Fig.6). The model is integrated in the ANSYS simulation platform. According to the conductivity and permeability of piece and the excitation frequency, the skin depth is 3 mm in the test piece. Therefore, four applications are processed in the framework of the project (fig.6).

**case 1:** Detection of open defects

**case 2:** Buired crack detection at a thickness of 2.5mm ( $e < \delta$ )

**case 3:** Detection of deep defects in a 15mm thickness ( $e > 3\delta$ ).

**case 4:** Detection of very deep defects at a thickness of  $e \gg \gg 3\delta$ .

These applications require the implementation of high sensitivity and high spatial resolution sensors to improve the signal to noise ratio and probability of detection. These cases demonstrate the need to test the performance of the inductive techniques studying the sensitivity of the coils as a function of the excitation frequency.

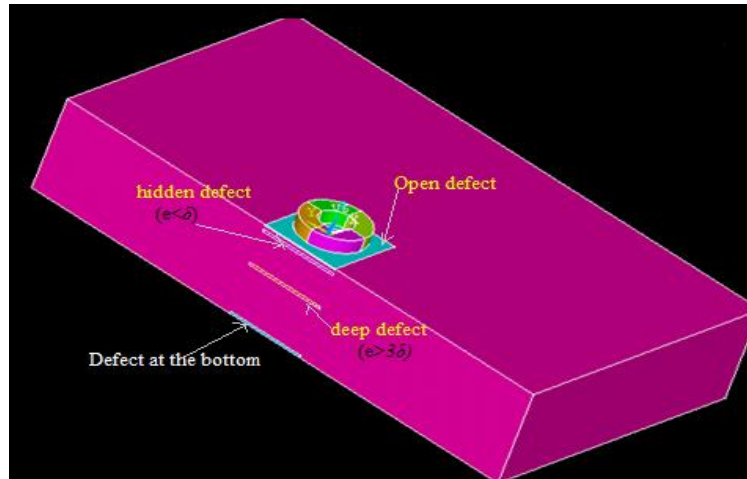


Fig.6: Planar configuration of open, buried, deep, defect and defect at bottom.

#### IV. Results And Discussion

##### Case 1: Detection of open defect

For the detection of open defects, results recommend the use of a high frequency eddy current sensor (several MHz).

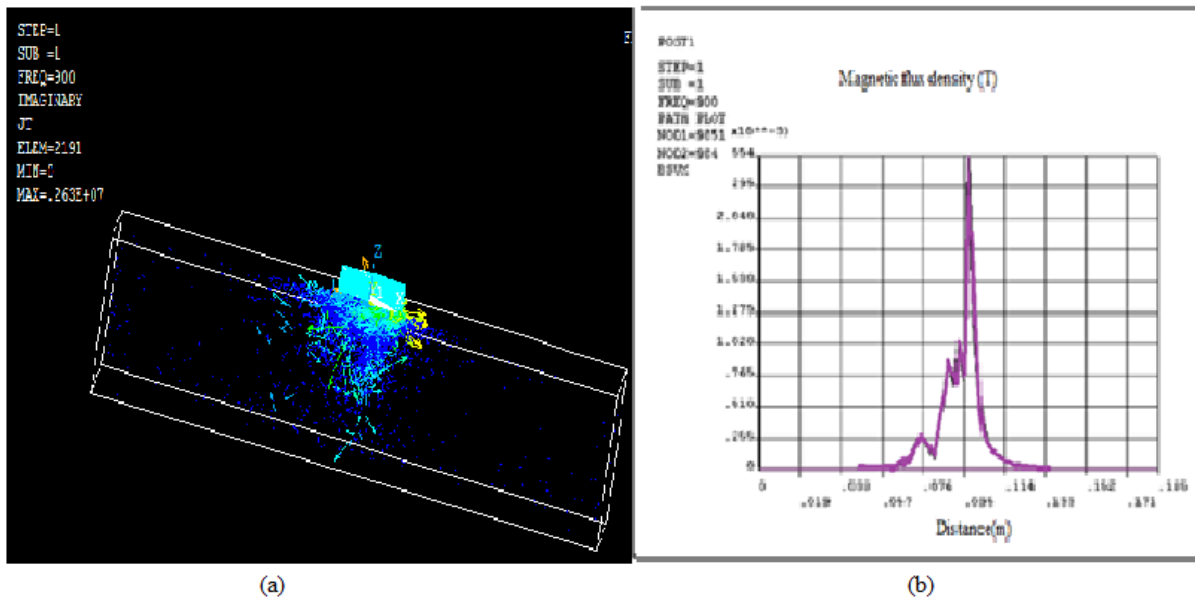
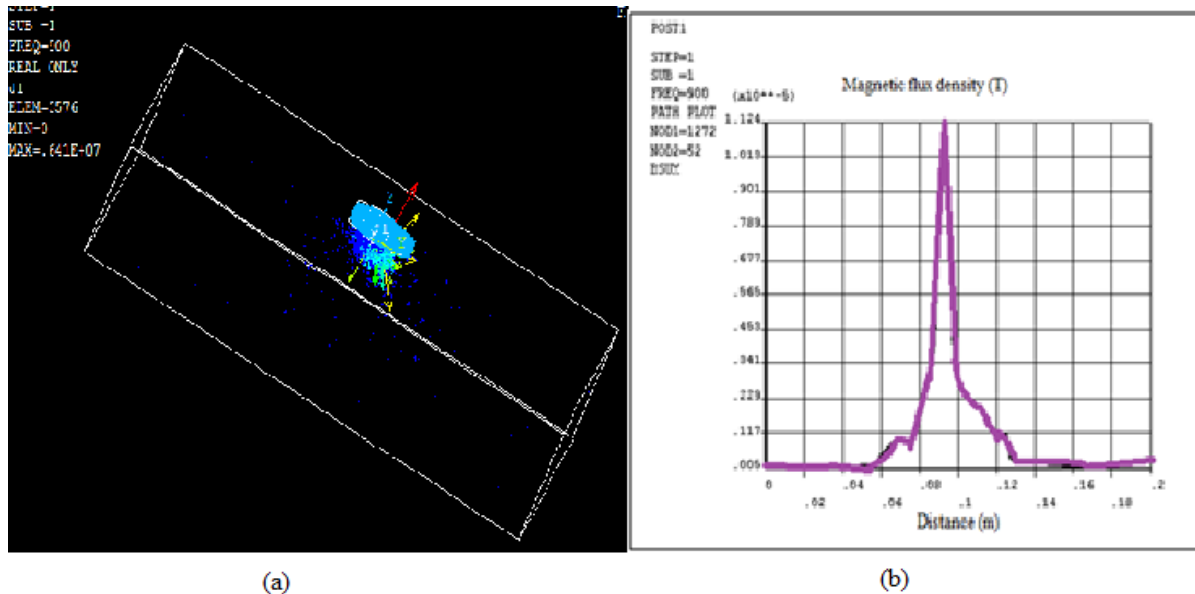


Fig.7: (a) Eddy current density distribution. (b) Variation of the magnetic flux linked to the open crack.

**Case 2: Detection of hidden defect ( $e < \delta$ )**

Regarding the detection of buried defects, simulation favors the use of a low frequency sensor (tens of Hz). We will use the same frequency as the first case.



**Fig.8: (a) Eddy current density distribution. (b) Variation of the magnetic flux linked to the presence of a hidden defect ( $e < \delta$ ).**

**Case 3: Detection of deep defect ( $e > 3 \delta$ )**

The eddy currents are located at shallow depth. This phenomenon is called skin effect, results in the difficulty or impossibility of detecting a defect located at a distance much greater than the skin depth  $\delta$ . Indeed, the eddy currents amplitude is less than 95% of the maximum amplitude beyond a depth greater than  $3\delta$ . In fig 9 the eddy current changes because of the crack and the magnetic flux increases in the defect zone which explains that the defect is clearly detected.

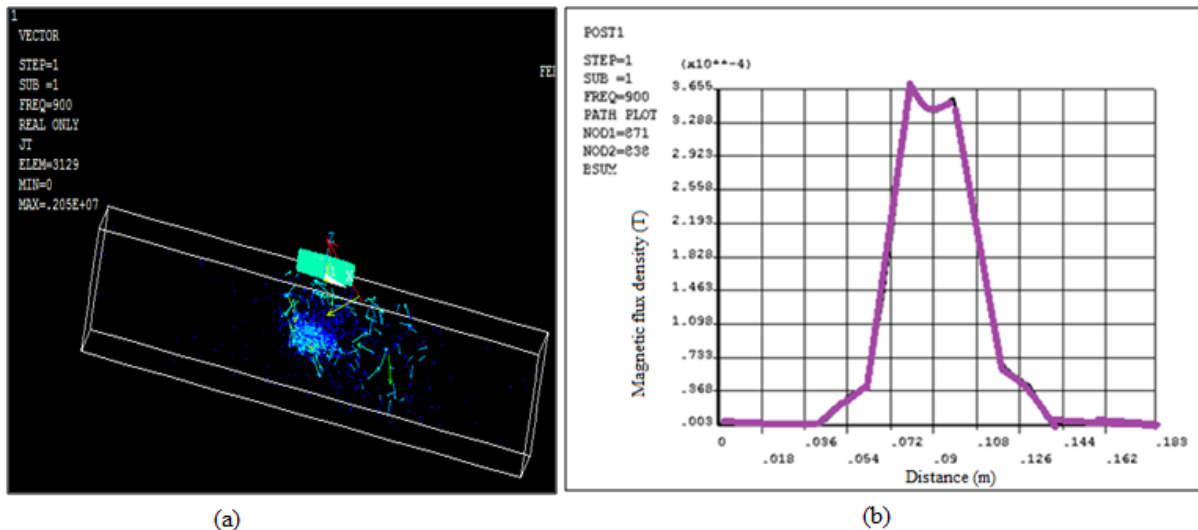


**Fig.9: (a) Eddy current density distribution. (b) Variation of the magnetic flux linked to the presence of a hidden defect ( $e > 3 \delta$ ).**

**Case 4: Detection of very deep defect ( $e \gg 3 \delta$ )**

The same behavior as the deep defect. ( $e > 3 \delta$ ), the defect at the bottom ( $e \gg 3 \delta$ ) which is so deep is also clearly detected despite the inability of eddy current sensors to detect defects at that depth.

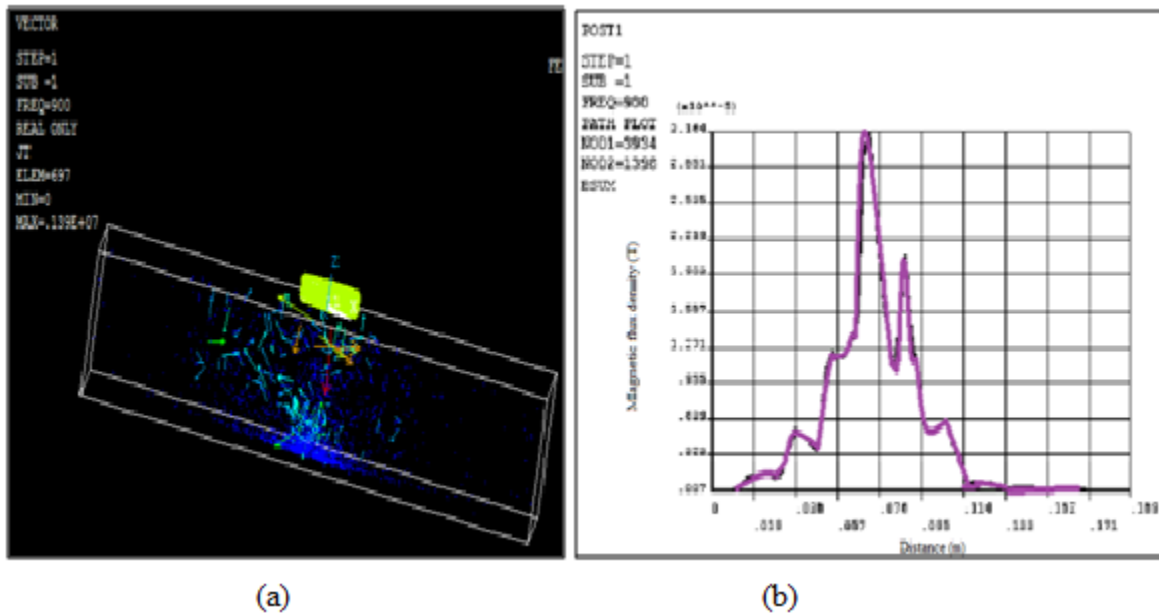


**Fig.10: (a)** Eddy current density distribution. **(b)** Variation of the magnetic flux linked to the presence of a defect at the bottom ( $e \gg 3 \delta$ ).

The results are presented in terms with the importance of the magnetic flux and eddy current density Fig.7-10 changes for all previous positions of crack. For the magnetic flux density the same behavior for the eddy current density that is important in the case of the open defect and decreases exponentially as a function of the depth of the target which is clear in the case of buried and deep defect. By contribution to what is said that this method is applicable to open defect and defects at shallow depths, we found that the deep defect will also mark and the distribution of the eddy current density shows the existence of the crack. Since the defect changes the field lines and the currents induced. The good agreement between signals validates the deep defect model.

## V. Conclusion

The numerical model developed makes it possible to simulate the variation of the impedance of a probe consisting currently by the transmitting / receiving coils, in the presence of a defect in a conductive medium. We presented simulation results and comparisons with data from the literature. Validation will be also extended to the case of a laminated plate can contain several defects. The prospects of this work are taken into account very deep flaws and detection enhancement for higher thicknesses to three times the depth of penetration.

## References

- [1]. S.Paillard, G.Pic "Development of a 3-D model for eddy current testing: Application for fastened structures in aeronautics" ,<hal-01104118>.. In proceedings of Cofrend conference. Cofrend 2008, May 2008, Toulouse, France.
- [2]. F. Foucher, X. Brunotte, A. Kalai, Y. Le Floch G. Pichenot, D. Prémel "Simulation of eddy current testing with civa and flux", In proceedings of Cofrend conference, Cofrend 2005, Beaune, France.
- [3]. M Mayos, M Lambert, C G-Pascaud, M Dessendre, N Dominguez, F Foucher, A Abakar "Groupe de travail COFEND sur la simulation des END par courants de Foucault Bilan d'activités",hal-01104115,V1, Jan 2016.
- [4]. A. Schumm, G. Pichenot, M. Mayos : "Simulation code validation targeting steam generator inspection with eddy current", 5th International Conference on NDE in relation to structural integrity for nuclear and pressurized components, San Diego, Mai 2006.
- [5]. L. Le Ber, P. Calmon, T. Sollier, S. Mahaut, P. Benoist : "Advances of simulation and expertise capabilities in CIVA platform", QNDE Vol. 25, 2006, pp. 684-691.
- [6]. H. Huang, N. Yusa, K. Miya- "Eddy current testing and sizing of fatigue",Asia-Pacific Conference on NDT, Nov 2006, Auckland, New Zealand.
- [7]. Le Ber L., Calmon P., Sollier T., Mahaut S. and Benoist P, "Advances of simulation and expertise capabilities in CIVA platform, in Review of Progress in QNDE" Vol. 25, 2006, pp.684-691.
- [8]. C. Zorni, C. Reboud, J.-M. Decitre et M. Lamber "Eddy current testing modeling of magnetic materialsDDY", Cofrend 2011 Dunkerque.
- [9]. M. Cacciola, S. Calcagno, G. Megali, F.C. Morabito, D. Pellicanò, M. Versaci, "FEA Design and Misfit Minimization for In-Depth Flaw Characterization in Metallic Plates with Eddy Current Nondestructive Testing". IEEE Transactions on Magnetics. 45(3) 2009, pp 1506-1509.

- [10]. T.Dogaru, .T.Smith,“Giant Magneto resistance Based Eddy-Current Sensor”. IEEE Transactions on Magnetics. 37(5), 2001, pp 3831-3838.
- [11]. T. Griesbach, M.C Wurz, L. Rissing, “Modular Eddy Current Micro Sensor”. IEEE Transactions on Magnetism. 47(10), 2011, pp.3760-3763
- [12]. M. Bensetti, Y. Choua, L. Santandrea, Y. Le Bihan, C. Marchand, “Adaptive Mesh Refinement and Probe signal Calculation in Eddy Current NDT Complementary Formulation”. IEEE Transactions on Magnetism. 44(6), 2008, pp.1646-1649.
- [13]. H. Huang, T. Takagia, T. Uchimoto “Fast numerical calculation for crack modeling in eddy current testing of ferromagnetic materials” J. Appl. Phys., Vol. 94, No. 9, Nov 2003, pp. 5866-5872. Japan.
- [14]. A.Zaoui, M.Feliachi, V.Doirat, M. Djennah, “A fast 3D modeling of arrayed eddy current sensor,” in Proceedings of the 12th Biennial IEEE Conference on Electromagnetic Fields Computation, CEFC-2006.
- [15]. R. Benlamine, F. Dubas, S-A. Randi, D. Lhotellier et C. Espanet Renault SAS “Méthode de Calcul Rapide des Pertes par Courants de Foucault dans les Aimants Permanents” France. <hal-01065266>Sep 2014.
- [16]. Ph. Beltrame and N. Burais, “Computing methods of hypersingular integral applied to Eddy-Current Testing,” IEEE Trans. Magn., vol. 38, pp.1269–1272, Mar. 2002.
- [17]. V.Ardon, O.chadebec, E.Clavel“Modélisation d’un capteur à courant de Foucault via un couplage de méthodes intégrale adaptées“. <hal-00472605> France. 2010.